Ultrasound in Med. & Biol., Vol. 32, No. 8, pp. 1247–1255, 2006

0301-5629/06/$–see front matter

ELSEVIER

doi:10.1016/j.ultrasmedbio.2006.05.004

● *Original Contribution*

A MODEL FOR REFLECTIVITY ENHANCEMENT DUE TO SURFACE BOUND SUBMICROMETER PARTICLES

Olivier Couture, Peter D. Bevan, Emmanuel Cherin, Kevin Cheung, Peter N. Burns, and F. Stuart Foster

Imaging Research, Sunnybrook Health Sciences Centre, Toronto, Ontario, Canada

(*Received* 19 *November* 2005, *revised* 18 *April* 2006, *in final form* 4 *May* 2006)

Abstract—Submicrometer particles filled with liquid perfluorocarbon have been shown to increase the ultrasound reflectivity of surfaces onto which they bind and, consequently, are seen as potential targeted contrast agents. The objective of this study is to explain the reflectivity enhancement as a result of the presence of randomly distributed particles on a surface. A model is presented where the diffraction-weighted scattering of all particles is summed over the exposed surface. Experiments were performed at frequencies ranging from 15 MHz to 60 MHz, with glass microbeads and perfluorohexane particles deposited on the surface of agar and Aqualene, a rubber closely matched to water, to confirm the validity of the model. Results showed that the model predicts the surface density and the frequency dependence of the reflectivity enhancement up to a density corresponding to twice the maximum packing of spheres on a surface (200% confluence fraction) for glass beads and a fifth (20% confluence fraction) for perfluorohexane particles. This suggests the possibility of predicting signal enhancement due to a bound contrast agent in simple geometries. (E-mail: olicou@swri.ca)

Key Words: **Ultrasound, Submicrometer particles, Perfluorocarbon contrast agent, Reflectivity, Bound particles.**

INTRODUCTION

Molecular imaging is directed at characterizing *in vivo* cellular and molecular processes, allowing better understanding and treatment of diseases (Weissleder et al. 2001). Different imaging modalities have shown potential for the visualization of biologic processes at the cellular level. In particular, ultrasound (US) (Dayton et al. 2002; Lindner 2004) has been considered for molecular imaging in applications related to the detection and characterization of atherosclerosis (Villanueva et al. 1998), inflammation (Lindner et al. 2000; Lindner 2001), angiogenesis (Ellegala et al. 2003), cardiac transplant rejection (Weller et al. 2003) and thrombus (Unger et al. 1998; Schumann et al. 2002). With US, the detection of microscopic biomarkers often requires the use of a highly echogenic contrast agent integrating an antibody or a ligand that will actively seek the target biomarker (Dayton et al. 2002). Although such contrast agents are, in general, microbubbles (Lindner 2004), liposomes (Demos et al. 1997) and submicrometer particles filled with liquid perfluorocarbon (Lanza et al. 1996) can be used as well.

Research to improve targeted US imaging has been mainly directed toward the enhancement of the echo from the contrast agent, the specificity of the targeted agent to the biomarkers and the agent stability *in vivo*. Moreover, the targeted contrast agents bound to a specific biomarker need to be differentiated from agent flowing in the blood. This was the early motivation for the use of liquid perfluorocarbon particles, which were shown to be poorly echogenic in blood (Hughes et al. 2005) but easily detectable when bound to a surface (Lanza et al. 1996). This phenomenon has been described over a wide range of frequencies and is of particular interest for high-frequency imaging of thrombus (Lanza et al. 1997) and possibly tumors (Hughes et al. 2004).

The high contrast between free-flowing and bound liquid perfluorocarbon particles has been explained by using a transmission line model, in which the particles were considered to form a layer of perfluorocarbon acting as a specular reflector when bound to a surface (Lanza et al. 1998; Hall et al. 2000; Marsh et al. 2002a; Marsh et al. 2002b). This model is simple and relatively

Address correspondence to: Olivier Couture, Imaging Research, Sunnybrook Health Sciences Centre, 2075 Bayview Avenue, 6th Floor, S wing, Toronto, Ontario, Canada, M4N 3M5. E-mail: olicou@swri.ca

accurate, but has been reported to underestimate the reflectivity enhancement of particles bound to a nitrocellulose membrane (Marsh et al. 2002b). Also, it does not take into account the particulate nature of the contrast agent, the density of its distribution on the surface, its size distribution or the particle scattering cross-section.

The approach taken here is to model the particles as a collection of individual scatterers all lying in the same plane. This approach could account for the nature of the surface and the nature of the particles, in particular their backscattering coefficient, and could include the effects of diffraction due to the geometry of the US source. The backscattering coefficient of perfluorohexane particles has been measured between 15 and 50 MHz in a previous study, which concluded that these particles act as linear Rayleigh scatterers (Couture et al. 2006). Using this information, we here develop and test a predictive model for the enhancement in the reflectivity when these particles are bound to a surface.

This study is an attempt to model the US reflectivity of submicrometer-sized particles bound to a surface through active targeting. Ultimately, our motivation is to improve the contrast using targeted contrast agents *in vivo*. However, to simplify the problem, model and experiments will concentrate on the effect of particles simply deposited on a surface. First, a model is presented that is based on scattering and diffraction theory. Second, experiments are performed using glass beads and perfluorohexane particles deposited on weakly reflective surfaces. The results of theoretical predictions are then compared with experimental measurement.

Theoretical model

A model to predict the reflectivity enhancement caused by particles targeted to a surface has been proposed (Lanza et al. 1998). In this model, the particles are viewed as a continuous film of perfluorocarbon covering the surface, with thickness corresponding to the particle diameter. The model is described by:

$$R(k) = R_{12} + \frac{T_{12}T_{21}R_{23}e^{2ikd}}{1 - R_{21}R_{23}e^{2idk}}, \qquad (1)$$

where R is the amplitude reflection coefficient at the interfaces between the film layer and the surrounding fluid or tissue, d is the film thickness and k is the wave number of the propagating US. R and T are the complex reflection and transmission coefficients at the different interfaces.

The model developed here considers a number of particles randomly and uniformly placed over a weakly reflective surface (Fig. 1). It is hypothesized that, at low surface concentration, the response can be modeled as the sum of the individual impulse response of all the particles, with all the phases accounted for. It is assumed

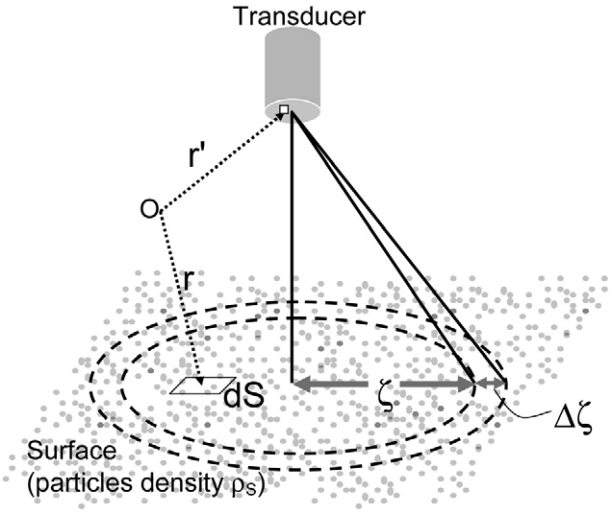

Fig. 1. Schematic for the proposed model. The particles are all lying in a plane. The contribution of the particles is summed over an annulus of width $\Delta\zeta$ at a distance ζ from the axis. Because the distance from the annulus to the transducer is a constant, the echoes from the particles in the annulus are all in phase.

that the increase of amplitude reflectivity from the particles can simply be added to the reflectivity of the surface itself. This assumption should hold if the particles are small enough and close enough to the surface for the interference between the scattered echo from a particle and the reflected echo from the underlying surface to be considered to be constructive.

The backscattering of particles randomly placed in space has been described extensively, in particular, in connection with speckle in organs (Foster et al. 1983; Shung et al. 1993), the echo from blood (Mo et al. 1992) and tissue backscattering (Madsen et al. 1984; Roberjot et al. 1996). The signal received at the transducer is often described by the convolution of diffraction, attenuation and scattering.

Madsen et al. (1984) describe backscattering from a collection of linear particles by summing their contribution over space, taking into account the frequency-dependency of backscattering and the phase from the two-way diffraction pattern, which can be calculated from the Rayleigh integral. The response is then corrected for diffraction and electromechanical response using the reflection from a quartz flat:

$$V_s(\omega) = \frac{1}{2\pi}\int_{T_1}^{T_2} dt e^{i\omega t}\int_{-\infty}^{\infty} d\omega'\, V_r(\omega)\left(R\iint_{S_{mir}} dsA_0(\mathbf{r},\omega')\right)^{-1} \times e^{-i\omega' t}\psi(\omega')\iiint_{Scatt.volume} d\mathbf{r}' N(\mathbf{r}')\left[A_0(\mathbf{r}',\omega')\right]^2 \quad (2)$$

where $V_S(\omega)$ is Fourier transformed and time-gated echo signal voltage. T_1 and T_2 are the time limits of the rectangular gating function. $V_r(\omega)$ is the echo signal from a reference reflector with amplitude reflection coefficient R.

$$A_0(\mathbf{r}, \omega) = \iint_S ds' \frac{\exp(ik|\mathbf{r} - \mathbf{r}'|)}{|\mathbf{r} - \mathbf{r}'|} \tag{3}$$

is related to the Rayleigh integral ($\mathbf{r}$ refers to the point where the pressure must be calculated and $\mathbf{r}'$ refers to the position of the source).

$$\iint_{S_{mir}} ds A_0(\mathbf{r}, \omega') \tag{4}$$

is the response from a transducer facing a perfect reflector. $\psi(\omega)$ is the square root of the differential scattering cross-section at π radian; $N(\mathbf{r})$ is the position of each scatterer. The triple integral is the sum over all scatterers in the observation volume corrected for two-way diffraction. For a concave transducer, $A_0(\mathbf{r}, \omega)$ can be calculated numerically by using the ring function method (Arditi et al. 1981; Fink et al. 1984). The differential scattering cross-section can be simulated from Faran's equations (1951). Finally, $V_r(\omega)$ is obtained experimentally.

If the particles are all located in the focal plane of the transducer, the volume integral is much simplified. The space dependence is reduced to a single variable ζ, which is the distance of the particles from the axis of the transducer. Because the phase of the particles sitting in an infinitesimal ring is uniform, one can calculate the volume integral in the following way:

$$\iiint_{Scatt.Volume} d\mathbf{r}' N(\mathbf{r}') \left[A_0(\mathbf{r}', \omega')\right]^2 = \int_0^\infty d\zeta 2\pi\zeta\rho_s \left[A_0(\zeta, \omega')\right]^2, \tag{5}$$

where ρ_S is the number of particles per unit surface. Note that it is a constant and can be taken out of the integral, indicating that the signal is proportional to the surface density of the particles. From this, an expression for the signal from particles randomly placed in a plane is obtained:

$$V_S(\omega) = \frac{\rho_S}{2\pi} \int_{T_1}^{T_2} dt e^{i\omega t} \int_{-\infty}^{\infty} d\omega' V_r(\omega) \left(R \iint_{S_{mir}} ds A_0(\mathbf{r}, \omega') \right)^{-1} \times e^{-i\omega' t} \psi(\omega') \int_0^\infty d\zeta 2\pi\zeta \left[A_0(\zeta, \omega')\right]^2. \tag{6}$$

Several assumptions are inherent in the model of eqn (6).

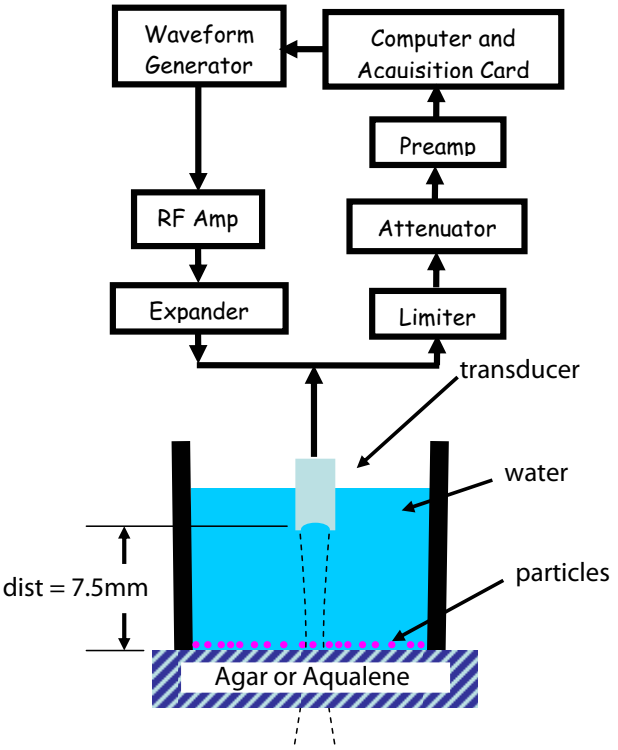

Fig. 2. Experimental set-up. A 50-MHz centre frequency transducer (7.5-mm focal length, f#2.5) is focused in the plane onto which the particles are deposited. A pulse-echo experiment is then performed to determine the reflectivity of the surface

First, the propagation and scattering of the US are assumed to be linear. It was also assumed that the echo from the particles and surface came from the same point in space. The surface density of the particles has to be low enough to exclude layering or ordered packing of the particles and multiple scattering. A minimal number of particles are also required for the phase of the wave scattered by the particles to be distributed uniformly. This statistical requirement also imposes a lower limit for the wavelength of the sound used in this model because a sufficient number of particles must be present within the beamwidth of the transducer.

Experimental method

In all experiments, the sample surface was immersed in water and placed at the focus of a 50-MHz broadband lithium-niobate transducer (7.5 mm focal length, 3-mm aperture), as shown in Fig. 2. A series of pulses of different frequency were emitted by an arbitrary waveform generator (AWG2020, Tektronix, Beaverton, OR, USA) and amplified by a power amplifier (M3206, AMT, Anaheim, CA, USA). Echoes reflected from the surface were collected, bandpassed filtered from 10 to 70 MHz, amplified by a 40-dB preamplifier (AU-

1313, Miteq, Hauppauge, NY, USA) and digitized (DP240, Acqiris, Geneva, Switzerland). Different narrow-band transmitted pulses (−6 dB bandwidth: 3 MHz) covering the range from 15 to 55 MHz were used. For each frequency, the transducer was positioned above 10 different regions 300 μm apart (about 1.2 times the −6 dB beamwidth at 15 MHz). At each transducer location, 100 pulses at a given frequency were transmitted and reflected echoes were acquired. Unless specified, the experiments were performed with pulse amplitudes at focus lower than 350 kPa peak-negative pressure.

At each transmitted frequency, the n echoes reflected from one region ($n = 100$) were averaged in time, as shown in eqn (7), Fourier-transformed and the signals from the m different regions ($m = 10$) were averaged in the frequency domain ($V_S(\omega)$ in eqn (6)). The parts of the spectra corresponding to the bandwidths of the pulses transmitted at each frequency were isolated and joined together to form a continuous frequency-dependent reflection amplitude curve. This curve was corrected for the transfer function of the transducer using the reflection from a quartz flat ($V_r(\omega)$ in eqn (6)) and the contribution of the underlying surface was subtracted in amplitude. The amplitude reflection coefficient of the surfaces was calculated from the comparison with the known amplitude reflection coefficient of the quartz surface. Unless specified, the data shown are the reflection coefficient or the normalized reflection amplitude at 40 MHz.

$$V(\omega) = \frac{1}{m} \sum_{m \ regions} \mathcal{F}\left[\frac{1}{n} \sum_{n \ pulses} s(t, m, n) \right]. \qquad (7)$$

Experiments were performed using glass beads 5.1 ± 0.5 μm in diameter (Duke Scientific Corporation, Palo Alto, CA, USA). The particles were mixed in water and placed in a sonic bath for 60 min to separate the beads. The solution was then poured in a container with Aqualene (Pulsecho Inc., Port Hope, Canada), a rubber of acoustical impedance very close to water, at the bottom. It was observed under light microscopy that beads sank in such a way that they were randomly distributed over the surface. Pulse-echo reflectivity measurements were performed when all the particles had sunk to the bottom surface (after 20 min). The surface density of the particles was calculated based on their number, mass and radius and this was then converted to a measure of confluence fraction, which represents the packing of the particles over the surface. A 100% confluence fraction is the highest possible packing of spheres in a plane, assuming a hexagonal distribution.

The production of perfluorohexane particles was described previously (Couture et al. 2006). Briefly, submicrometer droplets of perfluorocarbon were prepared by combining water, 5% v/v C_6F_{14} (FC72, 3 mol/L, St. Paul, MN, USA) and 0.2% v/v fluorinated surfactant (Zonyl FSO, Dupont Canada, Mississauga, ON, Canada). A coarse emulsion was obtained by mixing the solution for 1 min using a Vortex mixer. The coarse emulsion was then emulsified continuously for 3 min at a pressure of 100 MPa in a Microfluidizer (M-110EHI, Microfluidics, Newton MA, USA). The size distribution of the particles was estimated using dynamic light scattering (Nanosizer-S, Malvern Instruments Ltd, Malvern UK).

Because the submicrometer particles do not sink as fast as the glass beads, centrifugation was necessary. Sample preparation was performed in a 50-mL centrifuge tube partly filled with agar (0.5% to 5% m/v agar in water), molded to create a flat surface. The top part of the centrifuge tube was then filled with a solution of perfluorohexane particles in water. The tubes were centrifuged at 900g for 2 h before starting pulse-echo reflectivity measurements.

The assumption that all the particles sank to the surface was tested. Multiple pulse-echoes over the same regions were done before and after the addition of particles on top of the Aqualene surface. A second control experiment confirmed that the pulse pressure did not affect the particles. This was done using 1.6- and 8.3-MPa peak-negative pressure Gaussian 14-cycle pulses at 30 MHz (PRF 1 kHz) over one region. Finally, an experiment where the same concentration of particles was added over surfaces of different reflectivity (agar at concentrations ranging from 0.5% to 5%) was performed to verify the assumption that the amplitude reflectivity from the particles can simply be added to the reflectivity of the surface.

The expected reflectivity of the particles lying on a surface was calculated with the model of eqn (6), using the geometry of the experimental transducer, the reflection from the quartz flat and the expected backscattering coefficient of the particles obtained from the theory by Faran (1951). For particles with a broad-size distribution (polydisperse), the backscattering coefficient was calculated for all possible sizes of particles and weighted based on their size distribution measured by dynamic light scattering.

RESULTS

As shown in Fig. 3, the reflectivity of the Aqualene surface increased rapidly in the first 10 min after the addition of the glass microbeads in the water. It reached its maximum and stayed almost constant over the 1 h after the addition of the particles. Consequently, it was assumed that all the glass beads were sinking to the Aqualene surface and that the experiments could be performed 20 min apart. Moreover, considering that all the added particles ultimately ended up on the surface, the density of particles on the surface was calculated from the total mass of particles added.

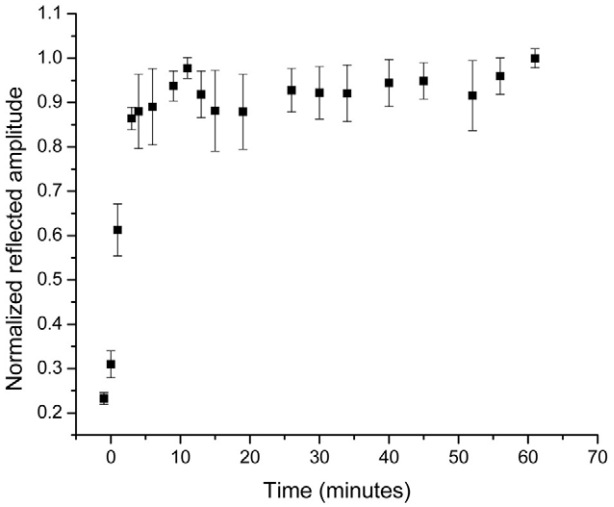

Fig. 3. Influence of the time-dependent accumulation of glass beads (on a surface of Aqualene) on the reflectivity. The error bars represent the standard error of trials done on different regions of the surface.

The results of the second control experiment, which tested the stability of the particles with respect to insonation pressure after they were deposited on the surface, are shown in Fig. 4. For this experiment, the lighter perfluorohexane submicrometer particles were used to highlight any effect of radiation pressure from the US beam. The reflection amplitude stayed unaffected, even after 5000 pulses at 1.6 MPa peak-negative pressure. Consequently, the particles were not likely be affected by the pulses at 350 kPa. However, at 8.3 MPa, the reflection amplitude decreased by 13% over the experiment.

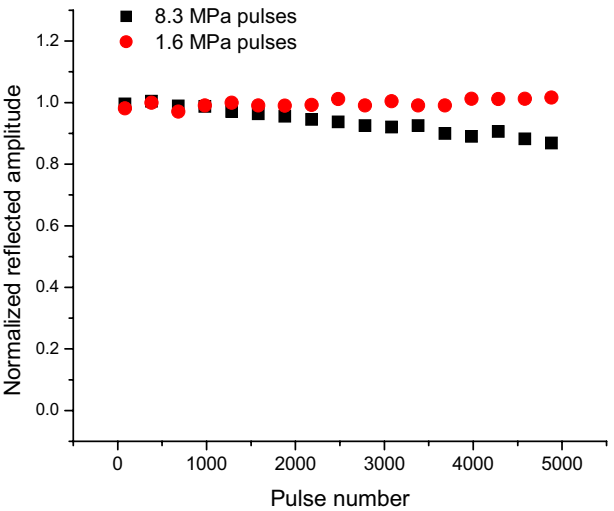

Fig. 4. Effect of high-power pulses on the reflectivity of perfluorohexane particles deposited on a surface. Icons are bigger than the error bars.

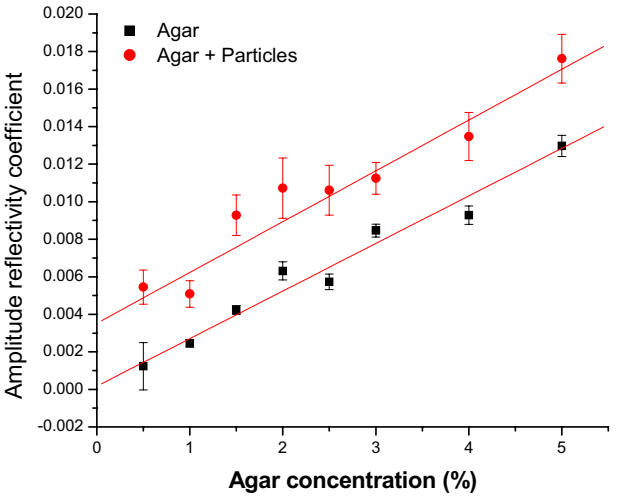

Fig. 5. Effect of a fixed amount of perfluorohexane particles deposited on surfaces of different concentrations of agar. The reflectivity coefficient of agar increases with a slope of 0.0025 ± 0.0001 and has a y-intercept of 0.00017 ± 0.00024 (r = 0.98). The reflectivity coefficient of agar with particles increases with a slope of 0.0027 ± 0.0003 and has a y-intercept of 0.0035 ± 0.0007 (r = 0.97). The error bars represent the standard error of trials done on different samples of agar.

The particles may have been displaced by radiation force or altered by the pulses.

The third control experiment verified the assumption that the contribution of the particles to the reflectivity could be added, in amplitude, to the reflectivity of the surface. The effect of adding a fixed amount of perfluorohexane particles (1.5 mL of original solution) over an agar surface (5.6 cm^2) made with varying concentrations of agar is shown in Fig. 5. The native reflectivity coefficient of agar increased fairly linearly with concentration, with a slope of 0.0025 ± 0.0001$\%^{-1}$ (r = 0.98). The reflectivity coefficient of agar with particles also increased fairly linearly, with a similar slope (0.0027 ± 0.0003$\%^{-1}$, r = 0.97). There was, however, higher variability in the reflectivity of the surface with particles, which was probably caused by inhomogeneities in the surface density of the particles. Because data were collected from 10 different uncorrelated regions, the mean was not strongly affected by this variability. The increase of the amplitude reflectivity coefficient of agar with particles was found to be linearly proportional to the increase of the reflectivity coefficient without particles (slope 1.0 ± 0.1, r = 0.97).

The effect of the accumulation of glass beads on the reflectivity of a surface of Aqualene is shown in Fig. 6. Figure 6a shows the entire span of the experiment and Fig. 6b zooms into the region of lower surface density. Until 200% confluence fraction, the reflectivity coefficient increased fairly linearly with the total number of

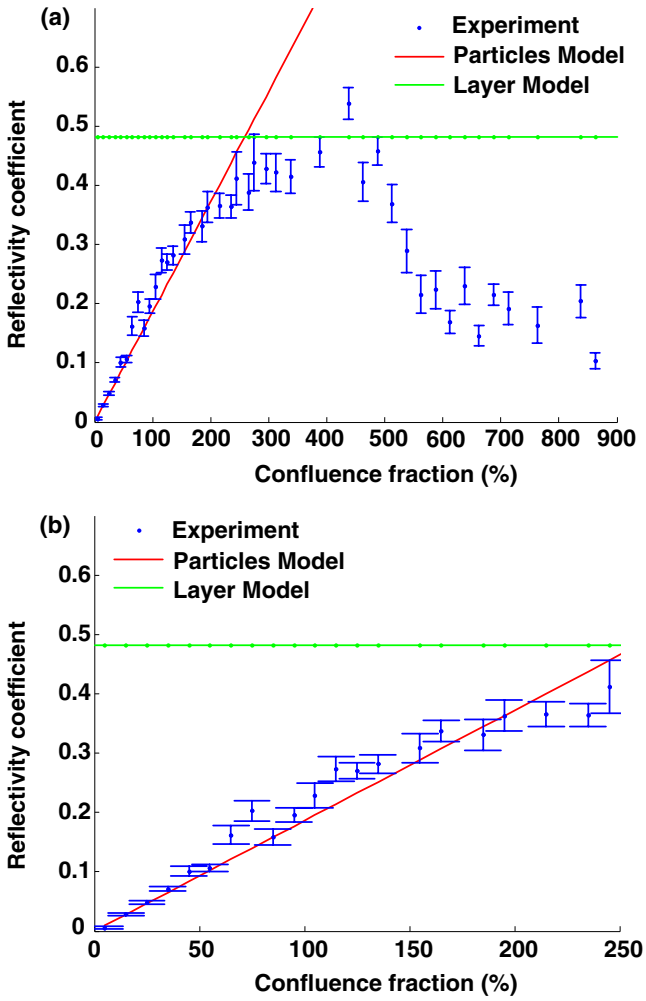

Fig. 6. (a) Variation of the reflectivity of a surface deposited with increasing number of glass beads (surface density dependence). (b) Until 200% confluence fraction, the reflectivity increases linearly with a slope of 0.00191 ± 0.0009 (r = 0.98). The error bars of Figs. 6, 7, 8 and 9 represent the standard errors of repeated trials over a surface.

particles (slope of 0.00191 ± 0.0009%$^{-1}$, r = 0.98). In the linear regime, the effect of the glass microbeads followed the particle model reasonably well. The transmission line model for a layer of glass of thickness corresponding to the diameter of the particles, which is surface-density-independent, predicted the peak value of the reflectivity. Beyond the linear regime, the reflectivity coefficient saturated and reduced to less than half the peak value around 600% confluence fraction.

The frequency dependence of the reflectivity coefficient at different confluent fractions is shown in Fig. 7. At lower confluence fraction (A, B), the reflectivity coefficient increased smoothly with frequency between 15 MHz and 55 MHz. The particle model was generally within error of the experimental results at confluence fractions lower than 150%. It deviated from a line for a confluence fraction around 300% (C), where it approached the prediction of the layer model. Although the transmission line model did not predict the actual value, it seemed to predict the shape of the frequency dependence over a wide range of surface density. At very high surface density (D), neither model predicted a frequency response that looked closer to an antiresonance pattern.

Figure 8 shows the effect of the accumulation of perfluorohexane particles (confluence fraction from 0 to 106%) on a 1% agar surface. The error was much larger than for experiments using microbeads. The reflectivity coefficient seemed to increase linearly until about 50% confluence fraction (fit, slope of 0.0009 ± 0.0001, r = 0.96). At very low confluence fraction (below 6%), the particle model fitted the experimental points. However, at higher confluence fraction, the model overestimated reflectivity enhancement. The transmission line model predicted the reflectivity for two values of confluence fraction. Figure 9 shows that only the particle model correctly predicts the frequency dependence of the reflectivity coefficient of the particles at lower confluence fraction.

DISCUSSION

The control experiments confirmed that the glass beads and the perfluorocarbon particles can be deposited on a surface of Aqualene or agar. Also, they showed that the particles are unaffected by the pulses used to interrogate their reflectivity. The third control experiment (Fig. 5) showed that the addition of particles did not change the slope of the increase of reflectivity caused by the increase in agar concentration. Consequently, if particles cover a weakly reflective surface, it is possible to sum their amplitude reflectivity to that of the surface itself. It can be argued that, since the top of the submicrometer particles is at a maximum distance of 1/40th of the wavelength from the surface (at 40 MHz), their reflections will probably interfere constructively with the surface. However, the additive rule is probably not as accurate for glass beads, which are bigger. Moreover, this simple addition does not take into account that the particles are probably shadowing part of the surface underneath. It was also not verified for surfaces with a high reflectivity because concentrations of agar higher than 5% were not found to be practical. However, the range may still be relevant for biologic medium modeling. As a comparison, a blood clot (density = 1.01g/cm^3, velocity same as water (Hall et al. 2001)) would have a reflectivity coefficient of 0.005 in water, whereas the most reflective surface in this experiment had a reflectivity coefficient of 0.012.

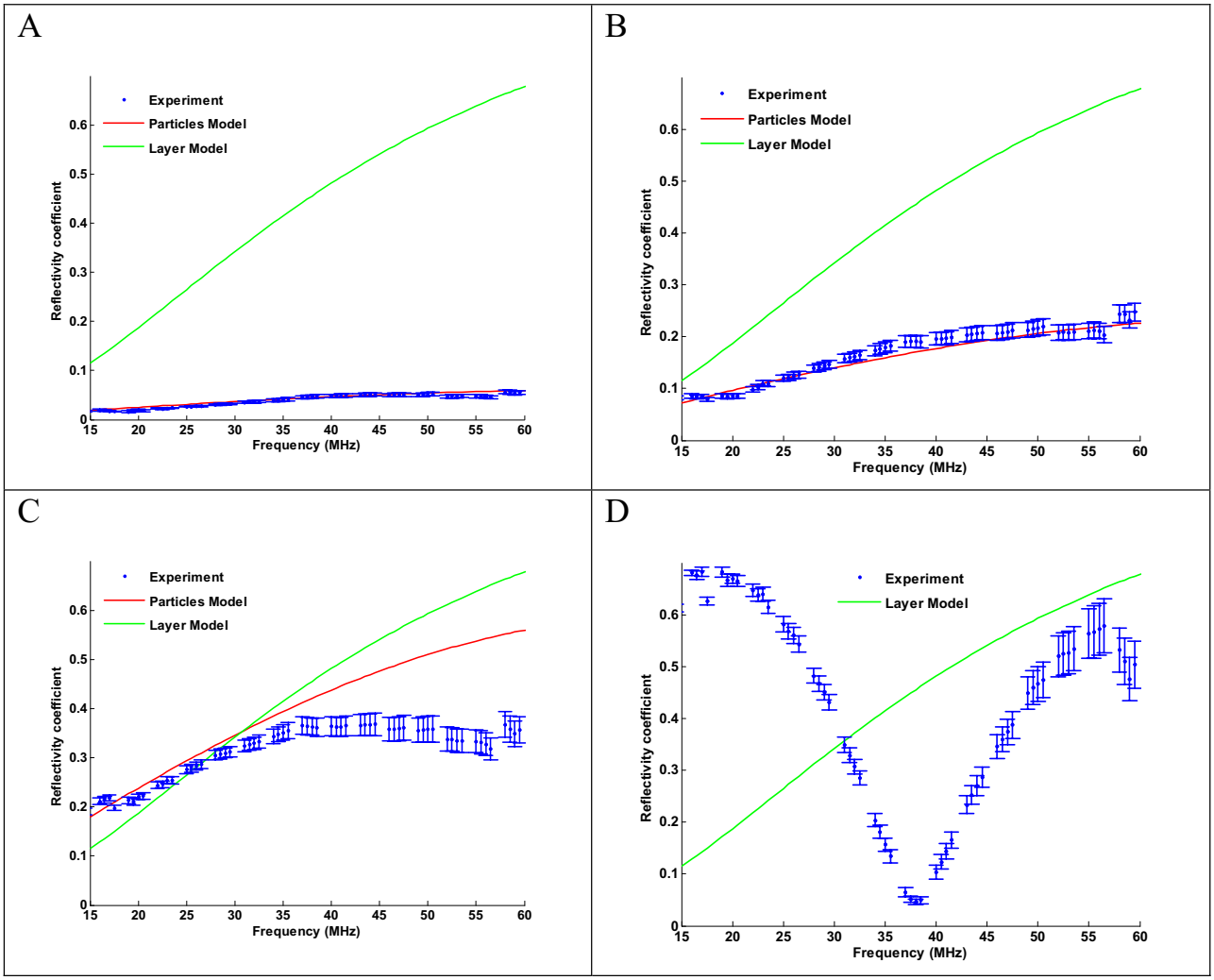

Fig. 7. Variation of the reflectivity of a surface deposited with increasing number of glass beads (frequency dependence). Confluence fraction (a) 25%, (b) 95%, (c) 235%, (d) 863%. In (d), the particle model is outside of the range of the graph.

Figure 6 shows that the reflectivity of glass beads on a surface increases linearly with number over a very wide range. The particle model predicts this proportionality, but not the transmission line model, which is independent of confluence fraction. It is surprising that the reflectivity coefficient increases linearly even over 100% confluence fraction. This result was not expected because particles were expected to start to pile up past that point and, consequently, to shadow each other's signals. The particle model followed quite accurately the experimental results in the linear region as shown in Fig. 6b. The transmission line model is independent of surface density and assumes a continuous layer, but it actually predicted quite accurately the maximum reflectivity of the particles over a surface (reflectivity coefficient of about 0.48).

It is interesting to note that Fig. 8 is similar to the curve of the backscattering from blood with increasing hematocrit (Mo et al. 1992). The reflectivity increased linearly with the number of particles until reaching a peak and subsequently decreased, possibly because the position of the scatterers was no longer random or the particles were pilling up and shadowing the particles underneath. The reflectivity coefficient of glass beads increased fairly smoothly with frequency for lower confluence fraction (<200%). However, interference-like behavior was observed at higher confluence fractions (>500 %). Over 800% confluence fraction, it showed complete cancellation at some frequencies. It is likely that the particles form a real layer, which would induce interference cancellation at certain frequencies.

In general, glass microbeads seemed to be ideal to confirm the model, because they were monodisperse (single size) and their number could be estimated from their total weight. Moreover, although the microbeads

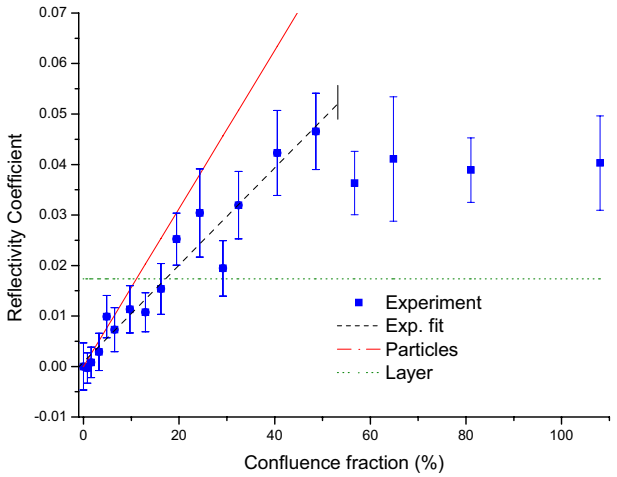

Fig. 8. Variation of the reflectivity of a surface deposited with increasing number of perfluorohexane particles (surface density dependence). The fit, which applies for confluence fractions below 50%, has a slope of slope of 0.0009 ± 0.0001 and a y-intercept of 0 .000 ± 0.003 (r = 0.96).

cannot be assumed to be pure Rayleigh scatterers at 40 MHz, their backscattering cross-section can be modeled using the theory by Faran (1951).

Transposing the model to the liquid contrast agent was more complex, because the perfluorohexane particles were polydisperse (mean Sauter diameter = 340 nm, FWHM = 200 nm). The expected response of each particle size had to be modeled, weighted with respect of their relative number and summed to obtain the total reflectivity coefficient. Nevertheless, Fig. 8 shows that the reflectivity still increases linearly with the number of particles, up to 50% confluence fraction. As expected from their impedance, the reflectivity coefficient caused by the perfluorohexane particles was lower than the one originating from glass beads (maximum around 0.045). It also saturates earlier. It is possible that the perfluorohexane particles have a tendency to interact with each other and do not act as independent scatterers beyond a certain density. As a comparison, note that reflectivity enhancement caused by perfluorohexane particles (50% confluence fraction) on a 1% agar surface is about 17 dB. This corresponds to the level of enhancement that has been reported in the literature and triggered the interest in these particles. The model predicts fairly well the reflectivity coefficient at lower confluence fraction (<5%). It also accurately follows the frequency dependence of the reflectivity. However, it overestimates the reflectivity at higher confluence fraction. This inaccuracy is probably caused by the fact that the model relies on an accurate measurement of the size of the particles, which could not be obtained. The transmission line model also predicts the reflectivity coefficient over a certain range. However, it does not follow the surface density or frequency dependence of the reflectivity.

These experiments showed that it is possible to represent the effect of particles of different composition, sizes and numbers deposited on a surface with a model summing their individual contributions. It may be used to predict the enhancement from targeted contrast agent in US imaging. The model, however, has several limitations. The assumed geometry, a plane, does not correspond to realistic *in vivo* imaging situations. To generalize to other geometries, the hypothesis of constructive interference between the particles and the surface would probably have to be abandoned. The particle model also assumes a random distribution of the scatterers with a known size distribution. Finally, the model does not work at very high concentrations of particles where piling, multiple scattering and organized distribution of scatterers become an issue. However, it is unlikely that confluence fraction higher than a few percent would ever be obtained *in vivo*.

This study shows that the reflectivity from a surface can be enhanced by the binding of particles up to a saturation concentration. Thereafter, the reflectivity cannot be increased by the addition of more particles, but only by increasing the backscattering cross-section of the particles, which is determined by their size and the acoustical properties of their content. Consequently, it may be preferable to use contrast agents with acoustical impedance very different from water, such as gas-filled agents. An additional advantage of using bubbles is their size-dependent resonance.

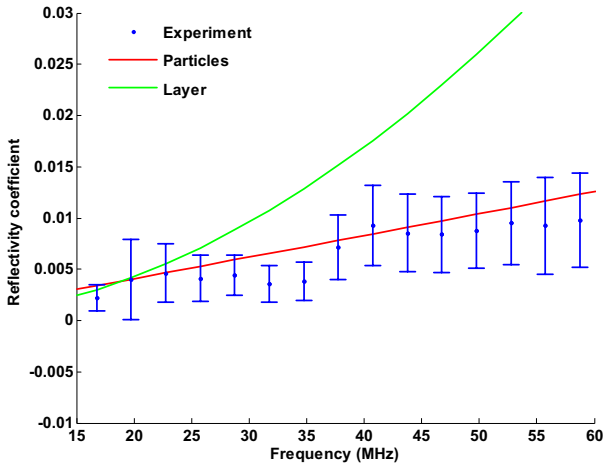

Fig. 9. Variation of the reflectivity of a surface deposited with increasing number of perfluorohexane particles. Frequency dependence at 4.8% confluence fraction.

CONCLUSION

This study showed that it is possible to deposit particles over a surface and to measure the US reflectivity enhancement. It also showed that the reflectivity of the particles could be added, in amplitude, to that of the surface. The frequency and confluence fraction dependence of the reflectivity coefficient could be predicted by using a model where the contribution of each scatterer weighted by the diffraction pattern of the transducer is summed. These experiments were performed for both monodisperse glass beads and polydisperse perfluorohexane particles. The particle model is more complex than previously described layer model, but yields more accurate predictions. The perfluorohexane particles are similar to contrast agents that have been proposed for targeted US imaging. This study may allow a better understanding of reflection enhancement caused by the accumulation of particles on a surface of the body such as the inner surface of an artery. The model should be extended to other geometries and other types of contrast agents with a linear or a nonlinear behavior.

Acknowledgements—We thank John Cannata for kindly providing an excellent 50-MHz lithium-niobate transducer. We also thank the Canadian Institutes of Health Research, the Ontario Research and Development Challenge Fund and the Terry Fox Programme of the National Cancer Institute of Canada for their funding.

REFERENCES

Arditi M, Foster FS, Hunt JW. Transient fields of concave annular arrays. Ultrason Imaging 1981;3:37–61.

Couture O, Bevan PB, Cherin E, et al. Investigating perfluorohexane particles with high-frequency ultrasound. Ultrasound Med Biol 2006;32:73–82.

Dayton PA, Ferrara KW. Targeted imaging using ultrasound. J Magn Reson Imaging 2002;16:362–377.

Demos SM, Onyuksel H, Gilbert J, et al. In vitro targeting of antibody-conjugated echogenic liposomes for site-specific ultrasonic image enhancement. J Pharm Sci 1997;86:167–171.

Ellegala DB, Leong-Poi H, Carpenter JE, et al. Imaging tumor angiogenesis with contrast ultrasound and microbubbles targeted to alpha. (v) beta3. Circulation 2003;108:336–341.

Faran JJ. Sound scattering by solid cylinders and spheres. J Acoust Soc Am 1951;23:405–418.

Fink MA, Cardoso J-F. Diffraction effects in pulse-echo measurement. IEEE Transact Sonics Ultrason 1984;SU-31:313.

Foster DR, Arditi M, Foster FS, Patterson MS, Hunt JW. Computer simulations of speckle in B-scan images. Ultrason Imaging 1983; 5:308–330.

Hall CS, Lanza GM, Rose JH, et al. Experimental determination of phase-velocity of perfluorocarbons: Applications to targeted Contrast Agent. IEEE Trans Ultrason Ferroelectr Freq Control 2000; 47:75–84.

Hall CS, Marsh JN, Scott MJ, et al. Temperature dependence of ultrasonic enhancement with a site-targeted contrast agent. J Acoust Soc Am 2001;110:1677–1684.

Hughes MS, Marsh JN, Allen JS, et al. In vivo ultrasonic detection of angiogenesis with site-targeted nanoparticle contrast agents using measure-theoretic signal receivers. Proceedings of the IEEE Ultrason Sympos 2004;2:1106–1109.

Hughes MS, Marsh JN, Hall CS, et al. Acoustic characterization in whole blood and plasma of site-targeted nanoparticle ultrasound contrast agent for molecular imaging. J Acoust Soc Am 2005;117: 964–972.

Lanza GM, Trousil RL, Wallace KD, et al. In vitro characterization of a novel, tissue-targeted ultrasonic contrast system with acoustic microscopy. J Acoust Soc Am 1998;104:3665–3672.

Lanza GM, Wallace KD, Fischer SE, et al. High-frequency ultrasonic detection of thrombi with a targeted contrast system. Ultrasound Med Biol 1997;23:863–870.

Lanza GM, Wallace KD, Scott MJ, et al. A novel site-targeted ultrasonic contrast agent with broad biomedical application. Circulation 1996;94:3334–3340.

Lindner JR. Assessment of inflammation with contrast ultrasound. Prog Cardiovasc Dis 2001;44:111–120.

Lindner JR. Molecular imaging with contrast ultrasound and targeted microbubbles. J Nucl Cardiol 2004;11:215–221.

Lindner JR, Dayton PA, Coggins MP, et al. Noninvasive imaging of inflammation by ultrasound detection of phagocytosed microbubbles. Circulation 2000;102:531–538.

Madsen EL, Insana MF, Zagzebski JA. Method of data reduction for accurate determination of acoustic backscatter coefficients. J Acoust Soc Am 1984;76:913–923.

Marsh JN, Hall CS, Scott MJ, et al. Improvements in the ultrasonic contrast of targeted perfluorocarbon nanoparticles using an acoustic transmission line model. IEEE Trans Ultrason Ferroelectr Freq Control 2002a;49:29–38.

Marsh JN, Hall CS, Wickline SA, Lanza GM. Temperature dependence of acoustic impedance for specific fluorocarbon liquids. J Acoust Soc Am 2002b;112:2858–2862.

Mo LY, Cobbold RS. A unified approach to modeling the backscattered Doppler ultrasound from blood. IEEE Trans Biomed Eng 1992;39: 450–461.

Roberjot V, Bridal L, Laugier P, Berger G. Absolute backscatter coefficient over a wide range of frequencies in a tissue-mimicking phantom containing two populations of scatterers. IEEE Trans Ultrason Ferroelectr Freq Control 1996;43:970–978.

Schumann PA, Christiansen JP, Quigley RM, et al. Targeted-microbubble binding selectively to GPIIb IIIa receptors of platelet thrombi. Invest Radiol 2002;37:587–593.

Shung KK, Thieme GA. Ultrasonic scattering in biological tissues. Boca Raton, FL: CRC Press; 1993.

Unger EC, McCreery TP, Sweitzer RH, Shen D, Wu G. In vitro studies of a new thrombus-specific ultrasound contrast agent. Am J Cardiol 1998;81:58G–61G.

Villanueva FS, Jankowski RJ, Klibanov S, et al. Microbubbles targeted to intercellular adhesion molecule-1 bind to activated coronary artery endothelial cells. Circulation 1998;98:1–5.

Weissleder R, Mahmood U. Molecular imaging. Radiology 2001;219: 316–333.

Weller GE, Lu E, Csikari MM, et al. Ultrasound imaging of acute cardiac transplant rejection with microbubbles targeted to intercellular adhesion molecule-1. Circulation 2003;108:218–224.